Backbone Dynamics of the A-Domain of HMG1 As Studied by ^{15}N NMR Spectroscopy†

R. William Broadhurst, Colin H. Hardman, Jean O. Thomas, and Ernest D. Laue*

Cambridge Centre for Molecular Recognition, Department of Biochemistry, University of Cambridge, Tennis Court Road, Cambridge CB2 1QW, U.K.

Received June 21, 1995; Revised Manuscript Received October 9, 1995⊗

ABSTRACT: The HMG-box sequence motif (~80 residues) occurs in a number of abundant eukaryotic chromosomal proteins such as HMG1, which binds DNA without sequence specificity, but with "structure specificity", as well as in several sequence-specific transcription factors. HMG1 has two such boxes, A and B, which show ~30% sequence identity, and an acidic C-terminal tail. The boxes are responsible for the ability of the protein to bend DNA and bind to bent or distorted DNA. The structure of the HMG box has been determined by NMR spectroscopy for the B-domain of HMG1 [Weir *et al.* (1993) *EMBO J. 12,* 1311−1319; Read *et al.* (1993) *Nucleic Acids Res. 21,* 3427−3436) and for *Drosophila* HMG-D (Jones *et al.* (1994) *Structure 2,* 609−627]. It has an unusual twisted L-shape, suggesting that the protein might tumble anisotropically in solution. In this paper we report studies of the A-domain from HMG1 using ^{15}N NMR spectroscopy which show that the backbone dynamics of the protein can be described by two different rotational correlation times of 9.0 ± 0.5 and 10.8 ± 0.5 ns. We show that the relaxation data can be analyzed by assuming that the protein is a rigid, axially symmetric ellipsoid undergoing anisotropic rotational diffusion; the global rotational diffusion constants, $D_{\parallel}$ and $D_{\perp}$, were estimated as 2.47×10^7 and 1.49×10^7 s^{-1}, respectively. By estimating the angle between the amide bond vectors and the major axis of the rotational diffusion tensor from the family of structures determined by NMR spectroscopy [see accompanying paper, Hardman *et al.* (1995) *Biochemistry 34,* 16596−16607], we were able to show that the ellipsoid spectral density equation can reproduce the major features of the ^{15}N T_1 and T_2 profiles of the three helices in the HMG1 A-domain. The backbone dynamics of the A-domain were then compared with those of the B-domain and the HMG box from HMG-D. This comparison strongly supported the differences observed in the orientation of helix I in the three structures, where the B-domain appears to be more similar to HMG-D than it is to the A-domain. These differences may turn out to be related to subtle differences in the DNA-binding properties of the A- and B-domains of HMG1.

The HMG box is a sequence motif of ~80 amino acid residues that occurs in two classes of chromosomal protein: relatively abundant proteins such as vertebrate HMG1 and yeast NHP6, which bind to DNA without apparent sequence specificity, and a class of transcription factors such as LEF-1 (lymphocyte enhancer factor-1) and SRY (the product of the mammalian sex-determining gene), which bind DNA sequence specifically. These proteins all bind to distorted or prebent DNA and are able to bend DNA. These properties reside in the HMG box. [For recent reviews of HMG-box proteins, see Ner (1992), Landsman and Bustin (1993), Grosschedl *et al.* (1994), and Baxevanis and Landsman (1995).]

We earlier determined the structure of the HMG-box motif in the B-domain of HMG1 (Weir *et al.*, 1993); the protein has a novel and distinctive twisted L-shaped structure with an angle of ~80° (defined as the angle between helices II/III) between the two arms (Weir *et al.*, 1993). Subsequently, another NMR[1] structure was reported (Read *et al.*, 1993) for the same domain, although as a 2-mercaptoethanol adduct, which had a similar fold but an angle between the arms of some 35° less, giving a more globular shape. [Read *et al.* (1993) quote an overall angle of 70° between helices I/II and helix III which compares with an angle of ~103° in our structure.] To determine whether, for example, the structures were flexible in solution, such that the angle between the arms varied, or whether the structures were genuinely different, we have studied the structure and backbone dynamics of the homologous A-domain of HMG1. In the accompanying paper (Hardman *et al.*, 1995) we describe the structure of the A-domain and show that it is very similar to our previous structure of the B-domain (Weir *et al.*, 1993) and the HMG box in HMG-D (Jones *et al.*, 1994). Here we present a ^{15}N NMR spectroscopic study of the dynamics of the backbone nuclei in the A-domain and compare the A-domain with the B-domain from HMG1 and the HMG box from HMG-D (Jones *et al.*, 1994).

The development of highly sensitive indirect detection experiments for studies of the backbone dynamics of ^{15}N nuclei (Nirmala & Wagner, 1988; Kay *et al.*, 1989) has made possible studies of the degree of internal motion of backbone amides as well as of the anisotropy of molecular reorienta-

† This work was supported by grants from the Science and Engineering Research Council/Biotechnology and Biological Sciences Research Council (BBSRC) of the U.K. to J.O.T. and E.D.L. and through support for the Cambridge Centre for Molecular Recognition by the BBSRC and the Wellcome Trust.

* Author to whom correspondence should be addressed.

⊗ Abstract published in *Advance ACS Abstracts,* December 1, 1995.

[1] Abbreviations: NMR, nuclear magnetic resonance; 2D, two dimensional; NOE, nuclear Overhauser effect; HSQC, heteronuclear single-quantum correlation.

0006-2960/95/0434-16608$09.00/0

tion. The relaxation data of the A-domain of HMG1 were analyzed using the model-free approach of Lipari and Szabo (1982) in a manner similar to that described for a study of the backbone dynamics of calmodulin (Barbato *et al.*, 1992). The results are consistent with our previously determined structures of both the B- and A-domains of HMG1 (Weir *et al.*, 1993; Hardman *et al.*, 1995) and the anisotropic tumbling in solution of a fairly rigid L-shaped protein.

MATERIALS AND METHODS

Preparation of Samples for NMR Spectroscopy. ^{15}N-labeled protein samples were prepared as described in the accompanying paper (Hardman *et al.*, 1995).

NMR Spectroscopy. NMR experiments for the A-domain were recorded under identical conditions, on samples of concentration ~2.5 mM (for experiments at a ^{15}N frequency of 50.7 MHz) or ~5 mM (for experiments at a ^{15}N frequency of 60.8 MHz), at pH = 5.0 and 25 °C, on Bruker AM500 and AMX600 NMR spectrometers. For the B-domain experiments a 1.0 mM sample was used, at pH = 5.0 and 20 °C; spectra were recorded at a ^{15}N frequency of 50.7 MHz on the AM500.

2D ^{1}H−^{15}N HSQC spectra to measure heteronuclear NOEs, T_1s, and T_2s were recorded, on a ^{15}N-labeled sample, essentially as described (Barbato *et al.*, 1992); spectra were acquired with a total of 128 (t_1) × 2048 (t_2) real points to give acquisition times of 71 and 127 ms in t_1 and t_2, respectively. For the A-domain, T_1 data points were obtained with ten different relaxation periods: 40.1, 80.1, 160.3, 300.5, 400.7, 601.0, 801.3, 1202.0, 1602.7, and 2003.3 ms. Ten delay times were also sampled in the T_2 experiments: 7.6, 15.2, 22.7, 37.9, 60.6, 75.8, 90.9, 128.8, 189.4, and 250.0 ms. For the B-domain, T_1 data points were obtained with nine different relaxation periods: 20.0, 100.0, 201.0, 301.0, 401.0, 501.0, 602.0, 702.0, and 802.0 ms. Eight delay times were sampled in the T_2 experiments: 8.5, 25.4, 50.9, 67.8, 93.3, 118.7, 144.2, and 169.6 ms. For the heteronuclear NOE experiments, the ^{1}H carrier was positioned on the water resonance, whose intensity was reduced by a 5 ms purge pulse before the beginning of the pulse sequence. All spectra were processed using the AZARA software package (W. Boucher, unpublished; available by anonymous ftp from ftp.bio.cam.ac.uk:pub/azara). The solvent signal was removed by convolution difference (Marion *et al.*, 1989), and linear baseline corrections were carried out in both dimensions. The spectra were analyzed and the line heights extracted using the ANSIG3 program running on a Silicon Graphics Indigo computer (Kraulis *et al.*, 1994).

RESULTS AND ANALYSIS

T_1, T_2, and NOE Relaxation Data for the A-Domain. We were able to measure line heights, free from the effects of overlap, for 68 out of a maximum of 77 peaks that were sufficiently well resolved in the 2D ^{1}H−^{15}N correlation spectra. The T_1 and T_2 data were fitted to a two-parameter exponential decay

$$I(t) = I(0)\exp(-t/T_i) \quad (i = 1, 2) \qquad (1)$$

using a Levenburg−Marquardt nonlinear least squares fitting routine (Palmer, 1991; Press *et al.*, 1986). Within the experimental error (see below), the decays were all satisfactorily monoexponential (data not shown). The NOE values were calculated according to the formula of Noggle and Schirmer (1971)

$$\mathrm{NOE} = (I' - I_0)/I_0 \qquad (2)$$

where I' is the intensity in the spectrum with presaturation and I_0 is the intensity in the control spectrum.

In an attempt to estimate the errors in the T_1, T_2, and NOE data, peak heights were compared in pairs of duplicate spectra acquired for the shortest relaxation delay used in both the T_1 and T_2 data sets. The uncertainty in peak height was taken to be the standard deviation of the differences divided by $\sqrt{2}$; the mean errors were estimated to be 1.8% and 6.0% for the T_1 and T_2 data sets, respectively. The same uncertainty in peak height was assumed for subsequent time points. These errors were larger than those estimated from the standard deviation of the noise (data not shown). Approximate peak height uncertainties for the NOE experiments were determined assuming the same mean percentage error as in the T_2 data divided by $\sqrt{2}$, because twice the number of scans were acquired. The errors in the determination of the T_1 and T_2 parameters were estimated by a Monte Carlo statistical method (Palmer, 1991). A total of 500 synthetic data sets were constructed according to a Gaussian distribution based on the experimental peak height as the mean and the uncertainty as the standard deviation. $I(0)$ and T_i were then obtained for each data set by least squares fitting, and the mean values and standard deviations were calculated from these data sets. We also estimated the errors in the determination of the T_1 and T_2 parameters from the covariance matrix (Zheng *et al.*, 1995) but found that this method gave 50% lower errors (data not shown). The measured T_1, T_2, and NOE data are summarized in panels a, b, and c of Figure 1, respectively; the actual values are given in the supporting information.

Analysis of the T_1, T_2, and NOE Relaxation Data for the A-Domain. Because the ^{1}H−^{15}N NOE is more sensitive to internal dynamics than the ^{15}N T_1 or T_2 (Kay *et al.* 1989), the effects of local motion within the A-domain of HMG1 are most evident from an analysis of the NOE data set (Figure 1c). When both dipolar and chemical shift anisotropy relaxation mechanisms are taken into account, the maximum calculated value of the NOE, at a ^{15}N resonance frequency of 50.7 MHz, and in the absence of rapid internal motions, is −0.18. The more negative values found toward the N- and C-termini reflect the increased importance of rapid internal motions in determining relaxation processes. The baseline regions in the NOE plot correspond to regions of well-defined secondary structure in the protein, namely, helix I (residues 14−28), helix II (38−50), and helix III (53−74). Larger negative NOE values indicate a substantial increase in local motions in the loop region between helices I and II. Notably, substantial internal motions are not seen in the loop between helices II and III or in the junction between the N-terminal extended strand and helix I.

Increased flexibility toward the termini and in the loop region is also indicated by a reduction in the rates of transverse and longitudinal relaxation, but these are superimposed on another effect that leads to larger baseline T_1 measurements and smaller T_2 values for helix III when compared with the other two. With the help of a plot of T_1 against T_2 (see Figure 2), residues can be classed into three groups. Group i has an average T_1 of ~620 ms and T_2 of

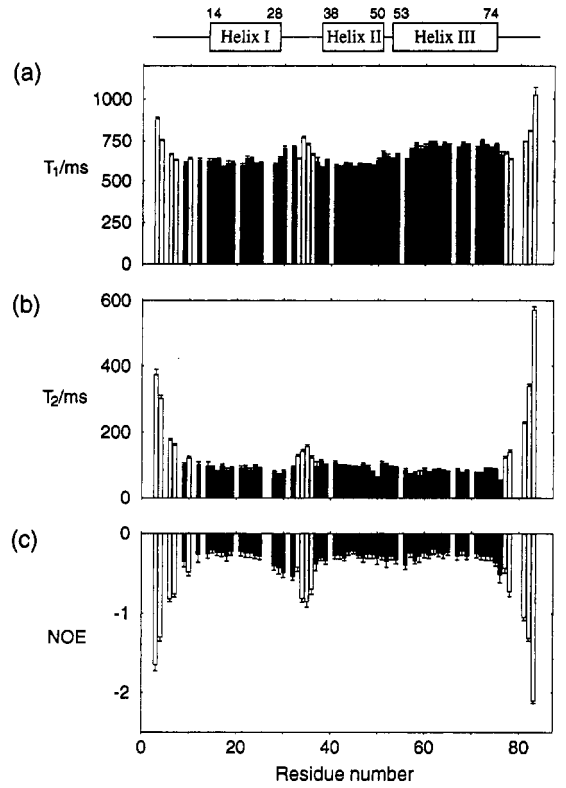

FIGURE 1: Plots of the ^{15}N T_1, ^{15}N T_2, and heteronuclear NOE (panels a, b, and c, respectively), recorded at a ^{15}N resonance frequency of 50.7 MHz, against the amino acid sequence for the A-domain of HMG1. Error bars, calculated using a Monte Carlo statistical method, are shown for each residue. Residues in groups i and ii are represented by shaded bars; see text for details.

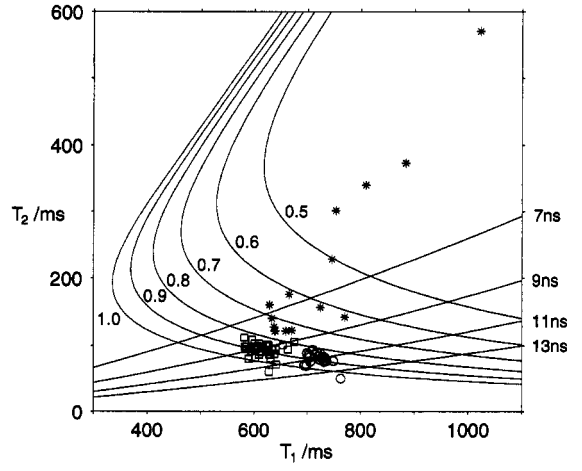

FIGURE 2: Plot of the experimental ^{15}N T_1 against the ^{15}N T_2 for the A-domain of HMG1. Each data point represents the values from a single amino acid residue; residues in groups i, ii, and iii are represented by squares, circles, and asterisks, respectively. Superimposed on the plot are two sets of contours based on the isotropic Lipari and Szabo spectral densities. The first set (labeled 0.5 → 1.0) shows how the order parameter S^2 affects the T_1/T_2 ratio as a result of changes in the rotational correlation time τ_m. The second set (labeled 7 → 13 ns) shows how the rotational correlation time τ_m affects the T_1/T_2 ratio as a result of changes in the order parameter S^2. For both sets of contours the internal correlation time τ_e was set to 50 ps.

~100 ms and includes 33 residues: 9, 12, 14−19, 21−25, 28, 29, 37−39, 41−54, and 56. Group ii has an average T_1 of ~720 ms and T_2 of ~80 ms and includes 18 residues: 57−65, 67−69 and 71−76. The remaining 17 residues are classed together in group iii: residues 3, 4, 6, 7, 10, 30, 32, 33−36, 66, 77, 78, and 81−83. When compared with the NMR structure (see accompanying paper and Figure 1), group i is found to be composed of residues from helices I and II, while group ii mostly consists of residues from helix III. Group iii contains all the flexible residues that give large negative NOE values at the N- and C-termini of the protein and in the loop region between helices I and II.

For an isolated $^1H-^{15}N$ spin system, the dipole−dipole and chemical shift anisotropy relaxation mechanisms give rise to the following expressions for the rates of longitudinal or transverse relaxation and the heteronuclear NOE (Wagner, 1993):

$$\frac{1}{T_1} = \frac{\hbar^2\gamma_N^2\gamma_H^2}{4r_{NH}^6}\{3J(\omega_N) + 6J(\omega_H + \omega_N) + J(\omega_H - \omega_N)\} + \frac{\omega_N^2\Delta_N^2}{3}\{J(\omega_N)\} \quad (3)$$

$$\frac{1}{T_2} = \frac{\hbar^2\gamma_N^2\gamma_H^2}{4r_{NH}^6}\{4J(0) + 3J(\omega_N) + 6J(\omega_H + \omega_N) + 6J(\omega_H) + J(\omega_H - \omega_N)\} + \frac{\omega_N^2\Delta_N^2}{3}\{^2/_3J(0) + {}^1/_2J(\omega_N)\} + R_{ex}^N \quad (4)$$

and

$$NOE = \frac{\hbar^2\gamma_N\gamma_H^3}{4r_{NH}^6}\{6J(\omega_H + \omega_N) + (\omega_H - \omega_N)\}T_1 \quad (5)$$

The analysis of the relaxation data is most easily achieved using the model-free approach of Lipari and Szabo (1982). They express the spectral densities $J(\omega_i)$, when $\tau_e < \tau_m$, as

$$J(\omega_i) = \frac{S^2\tau_m}{1 + (\omega_i\tau_m)^2} + \frac{(1 - S^2)\tau'}{1 + (\omega_i\tau')^2} \quad (6)$$

where S^2 is a generalized order parameter, τ_m is the correlation time for the overall motion, $1/\tau' = 1/\tau_e + 1/\tau_m$, and τ_e is an effective correlation time describing the rapid internal motions; if $S^2 = 1$, no internal motion occurs, but if $S^2 = 0$, more rapid internal motions dominate the relaxation. The above expressions for T_1 and T_2 [(3) and (4), respectively] can be reexpressed in terms of the Lipari and Szabo spectral density (6):

$$\frac{1}{T_i} = \frac{S^2}{T_i^{(0)}} + \frac{\hbar^2\gamma_N^2\gamma_H^2}{r_{NH}^6}(1 - S^2)\tau_e \quad (7)$$

where $T_i^{(0)}$, $i = 1, 2$, are the relaxation times for a macromolecule isotropically reorienting with correlation time τ_m. As S^2 becomes smaller, $1/T_1$ decreases due to the first term but increases due to the second. If the internal motion is very rapid, then

$$\frac{1}{T_i} \sim \frac{S^2}{T_i^{(0)}} \quad (8)$$

This shows that internal motion results in larger T_1 values

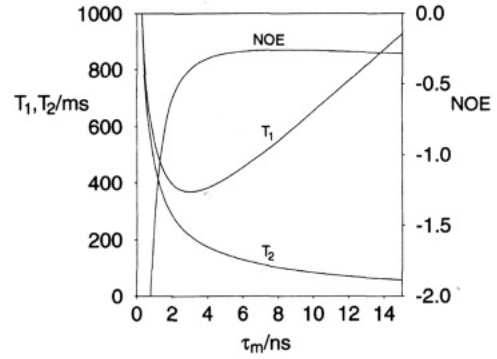

FIGURE 3: Plot showing the effect of the rotational correlation time τ_m on the ^{15}N T_1, ^{15}N T_2, and heteronuclear NOE assuming isotropic Lipari−Szabo model free parameters of $S^2 = 0.89$ and an internal correlation time $\tau_e = 50$ ps.

than would be expected for a rigid system. Similarly, internal motion causes T_2 to increase and the heteronuclear NOE to become more negative.

In Figure 2 we have included contours based on the Lipari and Szabo spectral densities to help gain a qualitative understanding of the information provided by the T_1 and T_2 experiments. The contour for order parameter $S^2 = 1.0$ forms a boundary for the data, showing the dependence of the longitudinal and transverse relaxation times on the global correlation time τ_m when internal motions have negligible effect. Data points close to the $S^2 = 1.0$ contour have been further classed together as group iv, comprising residues 29, 49, 50, and 76, since they all possess unusually large transverse relaxation rates, possibly due to contributions from conformational exchange on the millisecond time scale. (The model-free approach of Lipari and Szabo does not consider motions slower than the overall correlation time; these are usually dealt with using the R_{ex}^N term in eq 4.) When residues 29, 49, 50, and 76 are omitted, the mean T_2 changes from 93.4 ± 10.4 ms to 95.7 ± 7.3 ms for group i and from 79.1 ± 9.3 ms to 80.8 ± 6.2 ms for group ii; the corresponding mean T_1s are 615.6 ± 23.4 and 718.6 ± 15.4 ms for groups i and ii, respectively. The data values for groups i and ii are clustered around the contour for $S^2 = 0.9$, which is consistent with the idea that these residues probe a well-structured portion of the protein that allows little freedom for large amplitude internal motions on the sub-nanosecond time scale. All of the data points in group iii appear above the $S^2 = 0.8$ contour and therefore belong to more flexible regions of the protein. Figure 2 also shows that group i residues have data values surrounding the $\tau_m = 9.0$ ns contour, while the group ii points are closest to the $\tau_m = 11.0$ ns contour.

Determination of the Rotational Correlation Times. As shown (Kay *et al.*, 1989) for analysis of ^{15}N relaxation data according to the Lipari and Szabo model-free method, the mean value of the ratio T_1/T_2 can be used to estimate a global rotational correlation time, τ_m. Data from residues where either the NOE indicates that sub-nanosecond internal motions are significant, or the T_2s are anomalously short suggesting conformational exchange, are excluded from the analysis. Figure 2 shows that in the present case the T_1/T_2 profile is not consistent with a single rotational correlation time; when the data for groups iii and iv are omitted, the T_1/T_2 ratio suggests a τ_m of 9.0 ± 0.5 and 10.8 ± 0.5 ns for groups i and ii, respectively. As Figure 3 reveals, an increase in the overall rotational correlation time can account for

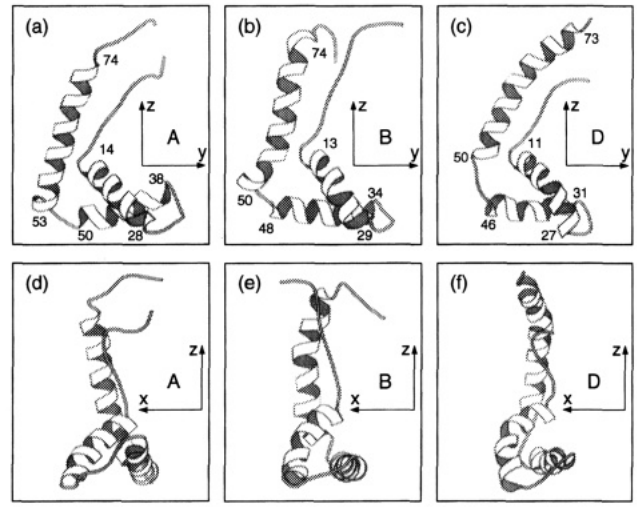

FIGURE 4: Structures closest to the mean of the moment of inertia for the families of (a) the HMG1 A-domain (Hardman *et al.*, 1995) designated A, (b) the HMG1 B-domain (PDB codes 1HME and 1HMF; Weir *et al.*, 1993) designated B, and (c) the HMG box from HMG-D (PDB code 1HMA; Jones *et al.*, 1994) designated D. In (d), (e), and (f) a different view, at right angles to those in (a), (b), and (c) respectively, is shown. The axes of the rotational diffusion tensor are also indicated and the structures are aligned such that the major axis of the moment of inertia lies along the z direction. Drawings were produced using MOLSCRIPT (Kraulis, 1991).

larger T_1 and smaller T_2 values for group ii relative to group i. The figure also shows that, at a ^{15}N resonance frequency of 50.7 MHz, the heteronuclear NOE is insensitive to changes in τ_m above 5 ns. This could explain why there is no significant difference in the baseline NOE values between the two groups; the mean NOE is −0.28 ± 0.05 and −0.26 ± 0.04 for groups i and ii, respectively.

Anisotropy of Molecular Tumbling in Solution. In the accompanying paper (Hardman *et al.*, 1995) we identified the different regions of secondary structure in the A-domain; groups i and ii consist of residues found in the well-defined α-helices. The tumbling of a protein in solution is characterized by a single rotational correlation time only if rotational diffusion is isotropic; an accurate description of anisotropic motion may need up to five correlation times (Woessner, 1962). The unusual structure of the A-domain from HMG1 lends support to the idea that it might tumble anisotropically. The protein is roughly cylindrical, with principal components of the diagonalized moment of inertia tensor in the ratio 2.5:2.0:1.0. The orientations of the principal axes are shown with a cartoon of the A-domain protein structure in Figure 4a,d. The largest component of the moment of inertia lies along the x axis, and this axis is roughly perpendicular to helices II and III, but at 45° to helix I. The next largest component is aligned along the y axis and is parallel to helix II, at 45° to helix I, and perpendicular to helix III. The z axis, about which overall rotation is fastest, is parallel to helix III, but nearly perpendicular to the other two. Figure 5a shows the direction cosines for the A-domain, calculated as an average over the family of NMR structures for all the backbone amide NH bonds. It has been pointed out (Barbato *et al.*, 1992) that the relaxation of a ^{15}N nucleus is not influenced by rotation about the NH bond vector but only by rotations that result in a change in the direction of the NH bond vector. Anisotropy of the overall motion of the protein is therefore expected to affect the spectral density function in a way that depends on the orientation of the NH

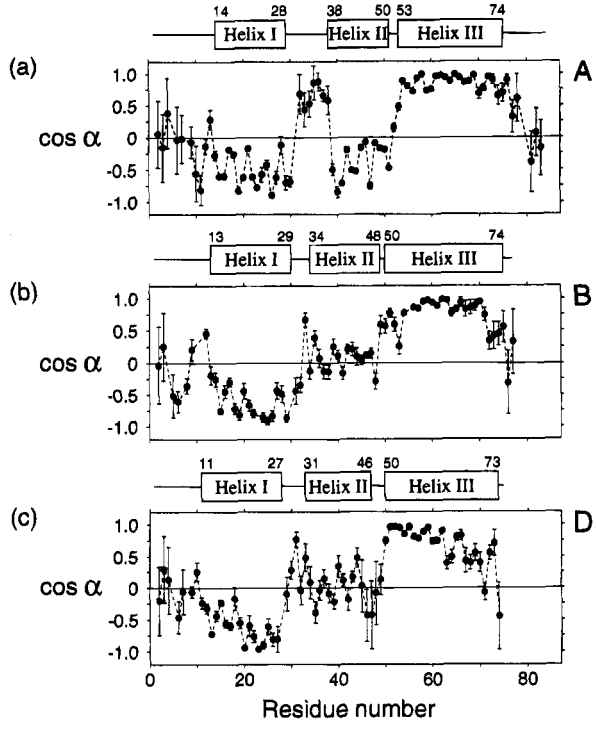

FIGURE 5: Plots of cos α (where α is the angle between the amide bond vector and the major axis of the rotational diffusion tensor) against the amino acid sequence for (a) the HMG1 A-domain (Hardman *et al.*, 1994) designated A, (b) the HMG1 B-domain (Weir *et al.*, 1993) designated B, and (c) the HMG box from HMG-D (Jones *et al.*, 1994) designated D. Each point represents the mean ± SD of cos α, relative to the major axis of the moment of inertia calculated for the sum of the family of structures aligned over the α-helices (see Figure 4). (It is likely that the direction cosines appear better determined in helix III because the cosine function is less sensitive to changes when α is close to 90°.)

bond vector relative to the principal axes of the molecular rotational diffusion tensor. Since the NH bond vectors in an α-helix are approximately parallel to the helical axis and helix III is roughly parallel to the axis about which overall rotation is fastest, it can be argued that the backbone amide ^{15}N nuclei of group ii are insensitive to this more rapid motion and so should have a longer rotational correlation time. Helices I and II are nearly perpendicular to helix III and should therefore experience the full effect of the rapid overall rotation, leading to a smaller τ_m value.

The Lipari and Szabo (1982) treatment of anisotropic overall motion yields a spectral density:

$$J(\omega) = \frac{2}{5}\left[S^2\left\{\frac{A\tau_1}{1+\omega^2{\tau_1}^2} + \frac{(1-A)\tau_2}{1+\omega^2{\tau_2}^2}\right\} + (1-S^2)\left\{\frac{A\tau_1 e}{1+\omega^2{\tau_{1e}}^2} + \frac{(1-A)\tau_{2e}}{1+\omega^2{\tau_{2e}}^2}\right\}\right] \quad (9)$$

where $1/\tau_{1e} = 1/\tau_1 + 1/\tau_e$ and $1/\tau_{2e} = 1/\tau_2 + 1/\tau_e$. The parameter A is similar in function to the order parameter S^2, scaling the overall correlation time between two values depending on the orientation of the NH bond. This expression has been used to investigate the likelihood of anisotropic tumbling in several studies, including those of ubiquitin and a peptide–calmodulin complex (Schneider *et al.*, 1992; Chen *et al.*, 1993). For example, in the study of ubiquitin a three-dimensional grid search was performed, fixing trial values of A, τ_1, and τ_2 for the whole system while optimum values of S^2 and τ_e were determined for each residue. A global error function was employed to indicate the best choice of A, τ_1, and τ_2. For ubiquitin, this method produced a minimum in the error function at $\tau_1 = \tau_2 = 4.1$ ns, with no unique minimum for the A parameter, indicating that the overall motion is isotropic. Although this result is reasonably correct for ubiquitin, which has principal components of the moment of inertia tensor in the ratio 1.6:1.4:1.0, the method is in general unlikely to uncover anisotropic rotational diffusion because it assumes A to be a global parameter rather than depending on the NH bond vector orientation of an individual residue. The approach will succeed only if most NH bond vectors have the same orientation. The disadvantages of employing this spectral density equation to investigate anisotropic motion are that it requires two global (τ_1 and τ_2) and three local (A, S^2, and τ_e) parameters, leaving the model undercharacterized for data acquired at one field, while the physical meaning of the correlation times τ_1 and τ_2 is not transparent.

More insight can be gained by assuming that the protein is a rigid ellipsoid undergoing anisotropic Brownian rotational diffusion in a continuous medium. In this way, an expression was derived (Woessner, 1962) for the spectral density that depends on the principal components of the rotational diffusion tensor and the orientation of the bond vector with respect to the axes of the ellipsoid. The further assumption that the ellipsoid has axial symmetry (and therefore possesses equal rates of diffusion about two axes) reduces the angle dependence to the magnitude of the component of the bond vector along the major axis. This idea was extended (Barbato *et al.*, 1992) to include internal motions after the manner of Lipari and Szabo (1982), giving

$$J(\omega) = \frac{2}{5}\left[S^2\left\{\frac{A_1\tau_1}{1+\omega^2{\tau_1}^2} + \frac{A_2\tau_2}{1+\omega^2{\tau_2}^2} + \frac{A_3\tau_3}{1+\omega^2{\tau_3}^2}\right\} + (1-S^2)\frac{\tau}{1+\omega^2\tau^2}\right] \quad (10)$$

where

$$\tau_1 = \frac{1}{4D_{\|} + 2D_{\perp}} \qquad \tau_2 = \frac{1}{D_{\|} + 5D_{\perp}} \qquad \tau_3 = \frac{1}{6D_{\perp}}$$

The form of this equation is similar to the previous one, but the theory now makes it clear that the rates of rotational diffusion parallel and perpendicular to the major axis determine the overall correlation times. If the internal correlation time τ_e is at least an order of magnitude smaller than τ_1, τ_2, or τ_3, then

$$\frac{1}{\tau} = \frac{1}{\tau_e} + \frac{1}{\tau_{m,eff}}$$

$$\tau_{m,eff} = \frac{1}{2D_{\|} + 4D_{\perp}}$$

The angle α between the NH bond vector and the major axis determines the extent to which each of the overall correlation times τ_1, τ_2, and τ_3 affects the relaxation via the scaling parameters A_1, A_2, and A_3:

$$A_1 = \frac{3}{4}\sin^4\alpha \quad A_2 = 3\sin^2\alpha\cos^2\alpha$$

$$A_3 = \frac{1}{4}(3\cos^2\alpha - 1)^2$$

Thus, an amide ^{15}N nucleus with its bond vector perpendicular to the major axis has relaxation properties determined by both $D_{||}$ and $D_\perp$, whereas a parallel bond vector leads to a dependence on $D_\perp$ alone. This model still has two global ($D_{||}$ and $D_\perp$) and three local (cos α, S^2, and τ_e) parameters, but the interpretation of all the parameters is now clear. If structural information is available, cos α can be estimated and the model fully characterized by data at just one field strength. A similar approach has been taken recently by others (Hansen *et al.*, 1994; Zheng *et al.*, 1995).

In the case of the HMG1 A-domain, the ratio of the principal components of the moment of inertia tensor (2.5:2.0:1.0) indicates that the symmetry of the protein is nearly axial. For lower symmetry, the principal axis system of the rotational diffusion tensor can be shifted from the moment of inertia axis system, especially for small molecules, due to interactions with solvent molecules (Dölle & Bluhm, 1989). However, the major axis of the rotational diffusion system coincides with that of the moment of inertia if the symmetry is axial or higher (Huntress, 1965). Recent molecular dynamics simulations show that proteins exhibit pure Debye rotational diffusion behavior, the size difference dominating any dipolar interactions between protein and solvent molecules (Smith & van Gunsteren, 1994). Consequently, the family of structures determined by NMR (Hardman *et al.*, 1995) was used to evaluate the average cos α for each residue with respect to the major axis of the moment of inertia. Figure 5a shows that residues in helix III have a mean cos α of 0.85 and are roughly parallel to the major axis, indicating that T_1 and T_2 values in this region of the protein are determined by the value of $D_\perp$, but are insensitive to $D_{||}$. Residues in helix I (mean cos α of 0.50) and helix II (mean cos α of 0.41) depend on both of the rotational diffusion rates.

Prediction of the Expected ^{15}N T_1/T_2 Profile Using the Ellipsoid Spectral Density Equation. Many previous studies of the ^{15}N relaxation of backbone amide nuclei have shown that, in regions of defined secondary and tertiary structure, the order parameter S^2 tends to have a uniform value and the correlation time for internal motion, τ_e, is very small. With this in mind, the underlying dependence of T_1 and T_2 on cos α should be revealed by assuming that the internal motions of all of the residues in the helices can be approximated by setting τ_e to zero and using an average value of S^2. In Figure 2, data points from residues within groups i and ii are distributed along the $S^2 = 0.9$ contour; this suggests that the longitudinal and transverse relaxation of these residues can be described by a single value of S^2, obtained using the isotropic Lipari−Szabo model if the overall correlation time τ_m is allowed free range between 8 and 12 ns. This approximation is equivalent to finding a unique τ_m for each residue that reproduces with a single Lorentzian, the sum of the three Lorentzians encountered in eq 10. A grid search was performed for residues in the three helices using the isotropic Lipari−Szabo model to find a global value of S^2 and the best local value of τ_m for each residue, yielding $S^2 = 0.89$. The rotational diffusion constants, $D_{||}$ and $D_\perp$, were then estimated from eq 10 by a two-dimensional grid search, fixing S^2 at 0.89, τ_e at 0, and using the mean local values of cos α from the family of structures for each amide NH bond vector. The global minimum was obtained with $D_{||} = 2.47 \times 10^7$ s^{-1} and $D_\perp = 1.49 \times 10^7$ s^{-1}. In order to understand the effects of the rotational diffusion constants, $D_{||}$ and $D_\perp$, on the range of possible ^{15}N T_1 and T_2 values, we also calculated the span of T_1 and T_2 values, for different values of the diffusion constants, assuming that the range of values of cos α for each amide NH bond vector was between 0 and 1, i.e., that α spans angles between 0° and 90° (relative to the major axis). In Figure 6, the dependence of the T_1/T_2 plot on the absolute value of $D_{||}$ and the ratio $D_{||}/D_\perp$ is shown. It is evident that the absolute value of $D_{||}$ determines where the range of allowed T_1/T_2 coordinates starts, whereas the ratio of $D_{||}/D_\perp$ determines the range of allowed T_1/T_2 values. Moreover, for the estimated rotational diffusion constants, the expected range of T_1 and T_2 values encompasses the range of experimental data from the structured residues in helices I, II, and III. Thus, having estimated the global parameters, these results demonstrate that the ellipsoid spectral density equation can reproduce the major features of the T_1 and T_2 profiles of the three helices of the HMG1 A-domain. In Figure 7, the best fit values of S^2 and τ_e for each residue, based on the mean value of cos α from the family of structures, are plotted.

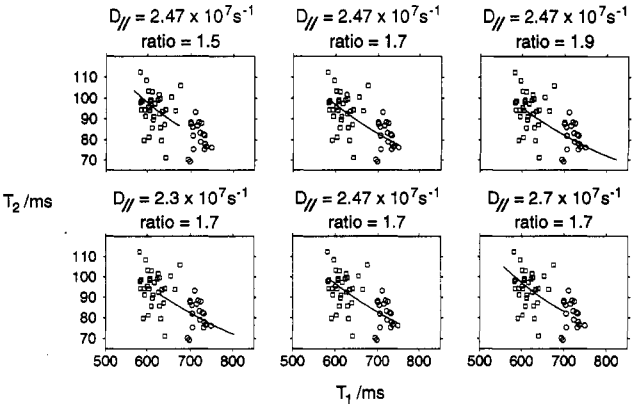

FIGURE 6: Plots showing the dependence of the ^{15}N T_1/^{15}N T_2 values on the absolute value of $D_{||}$ and the ratio of $D_{||}/D_\perp$ in the extended Woessner model; the top three panels illustrate the effect of $D_{||}$, whereas the lower three panels illustrate the effect of the ratio of $D_{||}/D_\perp$. The graphs are superimposed on the experimental ^{15}N T_1 and ^{15}N T_2 values for residues in groups i and ii (represented by squares and circles, respectively) of the HMG1 A-domain. The plots were generated by fixing S^2 at 0.89 and τ_e at 0 and assuming that the range of values of cos α for each amide NH bond vector is between 0 and 1, i.e., that α spans angles between 0° and 90° (relative to the major axis).

Comparison with Data Recorded at a Higher Field Strength. As an independent check of our results, we repeated all the measurements at a different field strength on a new protein sample which had a higher concentration. The results were very similar. In particular, the same trends in the baseline values of the T_1s and T_2s in helices I, II, and III were seen in the new data recorded at 60.8 MHz (data not shown, although the actual values are reported in Table 2 of the supporting information).

Comparison with the HMG box in HMG-D. We next compared our ^{15}N relaxation data for the A-domain with

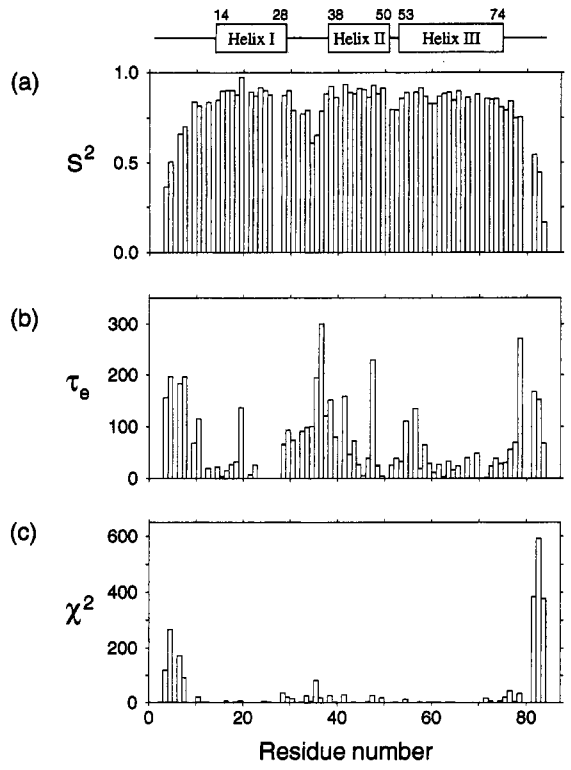

FIGURE 7: Plots of the best fit for the order parameter S^2, the internal correlation time τ_e, and χ^2 (the statistic for the fit) against the amino acid sequence for the A-domain of HMG1 (panels a, b, and c, respectively). The values were calculated from the experimental T_1 and T_2 data, using a Levenburg–Marquardt nonlinear least squares fitting routine, by putting the average values of cos α, obtained from the family of NMR structures, into the extended Woessner model, where $D_{\|} = 2.47 \times 10^7\ s^{-1}$ and $D_{\perp} = 1.49 \times 10^7\ s^{-1}$.

those for the HMG box from HMG-D (Jones *et al.*, 1994). Consistent with the very similar structures of the two HMG boxes (see accompanying paper), the similarity in the trends of the ^{15}N T_1s and T_2s is also very marked. In particular, increased T_1s and decreased T_2s are also observed for helix III (residues 50–73) in HMG-D, relative to the N-terminus of helix I and the whole of helix II (residues 11–~19 and 33–46 in HMG-D). Interestingly, however, in HMG-D there is a clear difference for the C-terminus of helix I (residues ~19–27 in HMG-D), in which increased T_1s and decreased T_2s similar to those in helix III are observed [see Figure 9 in Jones *et al.* (1994)]. These results strongly suggest a difference in the orientation of the C-terminus of helix I in the two proteins.

Figure 5 shows a comparison of the direction cosines, calculated for all the backbone amide NH bonds about the principal axis of the rotational diffusion tensor, for the A- and B-domains of HMG1 and the HMG box of HMG-D. In Figure 4, the structure closest to the mean of the moment of inertia for each of the three families is shown. Several differences between the A-domain and HMG-D are apparent. First, in HMG-D the C-terminus of helix III curves away from the major axis whereas in the A-domain it does not; otherwise, the angles between helices II/III are similar. Second, in HMG-D helix II is orthogonal to the major axis (the mean cos α is ~0) whereas in the A-domain it is at ~70° to the major axis. The most notable difference, however, is in the relative orientation of helix III and the C-terminus of helix I. Panels a and c of Figure 5 show that the mean cos α decreases toward the C-terminus of helix I in HMG-D, but not in the HMG1 A-domain. In the top views of the structures (Figure 4a, c) helix I is aligned similarly to helix III in both proteins, although helix I is seen to be slightly bent in HMG-D. In the lower views (Figure 4d, f) the orientation of the N-terminus of helix I is also similar; however, the C-terminus of helix I can now be seen to be almost aligned with helix III in HMG-D, but at ~45° to it in the A-domain. These observations are entirely consistent with the relaxation data which also suggest a similar relative orientation for the C-terminus of helix I and helix III in HMG-D.

Comparison with the B-Domain of HMG1. A plot of cos α against the amino acid sequence shows that the structure of the B-domain is more similar to HMG-D than it is to the A-domain (see Figure 5). This similarity is also very evident from the structures themselves, except that there is less of a curve in the C-terminus of helix III in the B-domain than in HMG-D (see Figure 4, c). However, the orientation at the C-terminus of helix I, relative to the major axis and helix III, is very similar (see Figure 4e, f). This prompted us to study the backbone dynamics of the B-domain of HMG1. The ^{15}N T_1, ^{15}N T_2, and $^1H-^{15}N$ heteronuclear NOE data of the B-domain show trends, in which the T_1s are increased and the T_2s are decreased for helix III (residues 50–71 in the B-domain), relative to some of the residues in helix I and the whole of helix II (residues 13–29 and 34–48, respectively, in the B-domain), that are very similar to those found for the A-domain and the HMG box of HMG-D. The observation of these trends, which we had also found in the A-domain (two independent sets of measurements) and which had been published for HMG-D (Jones *et al.*, 1994), convinced us that they were significant. In further support of this, we have also observed the same trends in both the A- and B-domains in the AB didomain (data not shown). However, as with HMG-D, in the B-domain the T_1s are increased and the T_2s are decreased toward the end of helix I (see Figure 8). We also noted a significant periodicity in the T_1s and T_2s in helix I; in general, larger T_1s and smaller T_2s are seen for residues on the inner side of the helix which packs against helix II (see Figure 8). This trend is mirrored in the cos α plot and, therefore, the structure; the NH bond vectors for residues on the inside of the helix tend to be aligned closer to the major axis and helix III (see Figure 5b), reflecting the fact that NH bonds are slightly out of plane and splay out at ~30° to the direction of the hydrogen bond and the helix (Baker & Hubbard, 1984). This trend is also apparent in the HMG box of HMG-D [see Figure 9 in Jones *et al.* (1994)]. The relaxation experiments, therefore, provide direct evidence for the differences seen in the three structures. The B-domain of HMG1 is evidently more similar to the HMG box of HMG-D than to the A-domain.

DISCUSSION AND CONCLUSIONS

Heterogeneity in the Structures of the A- and B-Domains of HMG1. The families of NMR structures of both the B- and A-domains of HMG1 (Weir *et al.*, 1993; Hardman *et al.*, 1995), showed symptoms of structural heterogeneity. In the B-domain structures we found that residues 10–61, consisting of helices I and II and the N-terminal half of helix III, are well defined. Likewise residues 5–10 and 63–73 together form a region that is well-defined locally. However, the mutual disposition of the two regions (10–61 and 5–10/

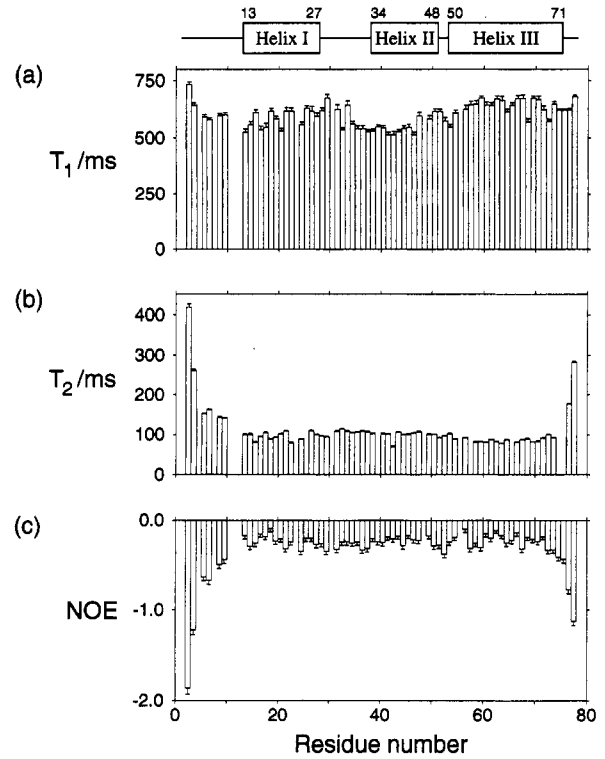

FIGURE 8: Plots of the ^{15}N T_1, ^{15}N T_2, and heteronuclear NOE (panels a, b, and c, respectively), recorded at a ^{15}N resonance frequency of 50.7 MHz, against the amino acid sequence for the B-domain of HMG1. Error bars, indicating the estimated errors in the measurements, calculated using a Monte Carlo statistical method, are shown for each residue.

63−73) is less well defined; in the 30 superimposed NMR structures after a least squares fit of residues 10−61, the end of the longer arm (residues 5−10/63−73) fanned out in a variety of directions. The reason for this is that the longer arm displays varying degrees of long-range bending between the different structures; similar effects are also seen when the structures are superimposed after a least squares fit of residues 5−10 and 63−73 (Weir *et al.*, 1993). Although this effect might have been due to insufficient experimental data in this region (some NOEs were unidentifiable in the spectra because of overlap), the structures suggested that there might be flexibility between the two arms. However, whether this was the case or not, the elongated shape of the molecule precluded better definition of the structure using essentially short-range and conservatively quantified NMR data (Weir *et al.*, 1993). Test calculations using a complete set of restraints derived from 1 of the 30 B-domain structures, classified in the usual way, showed that, even if we had been able to determine every possible restraint, NMR data of this precision could not uniquely define the overall conformation of the structure (Weir *et al.*, 1993). It follows that, even if there were substantial flexibility between the two arms, we would not have been able to detect it in the computed structures. In the NMR structures of the A-domain where we have determined a larger number of experimental restraints a similar, although not so dramatic, effect is seen. As discussed in more detail in the previous paper (Hardman *et al.*, 1995), we believe that this is due to the observation of longer range NOEs in the 3D/4D ^{13}C-separated NOESY spectra of the A-domain.

Understanding the Unusual ^{15}N T_1/T_2 Profile of the A-Domain. The ^{1}H−^{15}N NOE data of the A-domain of HMG1 suggest that residues in the loop between helices II and III, and in the junction between the N-terminal extended strand and helix I, are not flexible on the subnanosecond time scale. In a study of the backbone dynamics of calmodulin, the T_1/T_2 profile was also found to have a bimodal distribution, leading to predictions of a mean τ_m of 4 and 3 ns, for residues in the N- and C-terminus of the protein, respectively (Barbato *et al.*, 1992). In that study, however, the ^{1}H−^{15}N NOE data showed that the protein consists of two domains of different sizes that are connected by a linker region, flexible enough to permit independent rotational diffusion. This is not seen in the A-domain. Although there is some evidence for conformational flexibility (residues 16, 49, 50, and 57 have somewhat lower T_2s, indicative of some small amount of conformational exchange on the millisecond time scale), the residues in the elbow of the HMG domain clearly do not act as a flexible tether between the two arms of the L-shaped structure as suggested (Falciola *et al.*, 1994).

We wondered, however, whether the unusual T_1/T_2 profile observed for the A-domain could be attributed to a somewhat less flexible structure having more widespread, but slower, motions. In a study of the (30-51) folding intermediate of BPTI, the T_1/T_2 ratio was also far from constant (van Mierlo *et al.*, 1993) and could not be used to provide a characteristic overall correlation time. This behavior was attributed to widespread slow internal motion on the 1 ns time scale, which rendered T_1 insensitive to changes in the order parameter. More recently, Jones *et al.* (1994) have described ^{15}N relaxation studies of the HMG box in HMG-D. They also found that the T_1/T_2 ratio was far from constant and suggested that substantial exchange contributions in the C-terminus of helix I and all of helix III were needed to explain the lower T_2 values found for these regions. Changes in local structure could lead to line broadening in the ^{15}N spectrum if the rate of exchange is similar to any differences in ^{15}N frequencies between conformers. For the A-domain the T_2 values of group ii are indeed smaller than those of group i, but conformational exchange should only affect transverse relaxation times and cannot account for the concomitant increase in T_1 values observed in group ii. Jones *et al.* also found larger T_1 values for those residues displaying rapid transverse relaxation in HMG-D and found it necessary to lower the order parameter in these regions; the effect of a lower S^2 would be to increase both T_1 and T_2, but overall the T_2 would be lowered due to the exchange contributions. In the case of the A-domain, the increased T_1 values of group ii are close to those found in the flexible loop region between helices I and II. If there is a similar contribution of subnanosecond local motion to the lontitudinal relaxation rate of residues in group ii, this ought to be apparent in the profile of the NOE data in Figure 1c. However, NOE values for group i residues are very similar to those of group ii, ruling out this interpretation of the data. Furthermore, there is no reason why conformational exchange should only affect residues in group ii; some residues in group i would be expected to be similarly affected.

The difference in the T_1 baseline between groups i and ii could in principle be attributed to a change in the time scale of internal motions that are faster than the overall correlation time. To help understand how the ^{15}N T_1 and T_2, as well as the heteronuclear NOE, are affected by a change in the time scale of local motions, the effects of changes in the order

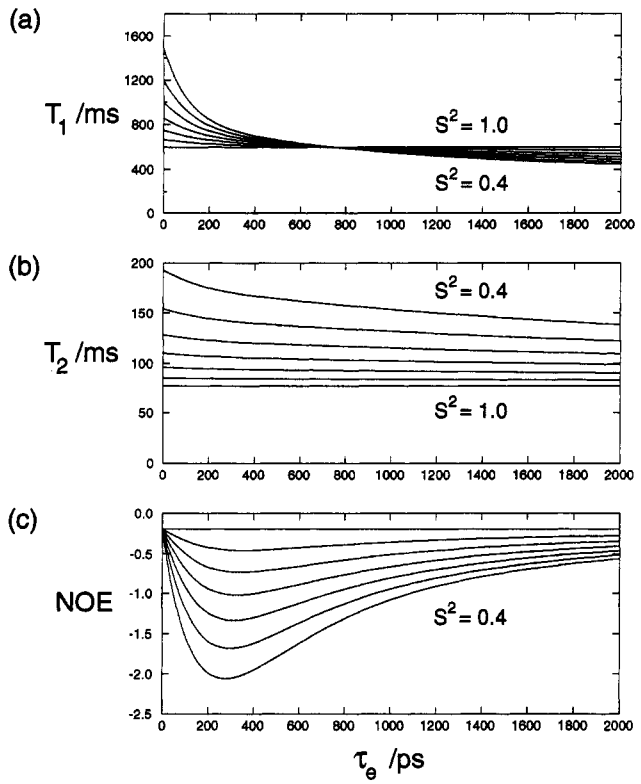

FIGURE 9: Plots showing the variation of the ^{15}N T_1, ^{15}N T_2, and heteronuclear NOE (panels a, b, and c, respectively) when the order parameter S^2 is set to 1.0, 0.9, 0.8, 0.7, 0.6, 0.5, and 0.4 and the rotational correlation time τ_m is fixed at 10 ns.

parameter, S^2, and the effective correlation time for the internal motions, τ_e, are plotted in Figure 9. Figure 9a shows that, if we assume that S^2 is the same for both groups (see Figure 7), motions in group ii would have to be more rapid than those in group i in order to give the experimentally observed increase in T_1 for group ii. However, the same conditions also demand a large difference in the NOE baseline between the two groups (see Figure 9c) and that T_2 values for group ii are slightly larger than those of group i (see Figure 9b). Neither of these predictions is supported by the data, also ruling out this interpretation.

In passing, it is worth noting how Figure 9 reveals the effect of changes in the model-free parameters on ^{15}N relaxation effects, as also discussed by others but from a different viewpoint (Clore *et al.*, 1990; van Mierlo *et al.*, 1993; Eriksson *et al.*, 1993; Fushman *et al.*, 1994; Borer *et al.*, 1994). When the overall correlation time is 10 ns, T_2 is not very sensitive to the time scale of internal motions but is a good measure of the order parameter (Figure 9b). T_1 is most affected by very rapid local motions, but as mentioned above, the effect decreases as τ_e increases, passing through a null at around 750 ps. For longer time scales, local motion decreases the longitudinal relaxation time, in contrast to the increase found for small τ_e values. The heteronuclear NOE is not affected by the fastest internal motions but is most sensitive when τ_e is close to 300 ps. Clore *et al.* (1990) extended the Lipari−Szabo model to allow for internal motions on two different time scales in order to explain cases where the original three-parameter model could fit the T_1 and T_2 data accurately but predicted NOE values more negative than those observed by experiment. The internal correlation time τ_e was replaced by two time constants for slow and fast local motions, τ_s and τ_f, respectively, while an extra order parameter S_f^2 was introduced to describe the relative contributions of the two motions. However, modifying S_f^2, τ_s, or τ_f causes both T_1 and T_2 to change in the same direction, so the extended model cannot account for baseline T_1 and T_2 values changing in opposite directions as we find for groups i and ii.

A further, perhaps more unlikely, explanation for the T_1/T_2 profile observed for the A-domain is that the amide bond lengths differ systematically between residues in groups i and ii. However, an examination of eqs 3 and 4 reveals that such a difference would be expected to affect both T_1 and T_2 in the same sense, similar to a change in the time scale of internal motions.

In summary, having eliminated explanations based on different amide bond lengths, conformational exchange, variations in internal correlation times, and the extended Lipari−Szabo model, the results suggest that the difference in relaxation properties between groups i and ii is not the result of a widespread change in the nature of the internal motions of, say, helix III compared with helices I and II. It seems more likely that the spread in the families of NMR structures of both the B- and A-domains is, as originally suggested (Weir *et al.*, 1993), due to the elongated shape of the molecule in which better definition of the structure is precluded when using only essentially short-range and conservatively quantified NMR data.

The simplest interpretation of the two clusters seen in Figure 2 is that group i and group ii are described by different rotational correlation times. When the group (iv) residues are omitted, the T_1/T_2 ratio suggests a τ_m of 9.0 ± 0.5 and 10.8 ± 0.5 ns for groups i and ii, respectively. These two mean τ_m values are separated by more than two standard deviations, and it is very unlikely that this could be attributed to statistical error. We repeated the experiments at a higher field strength to strengthen further this conclusion. By making the reasonable assumption that the protein is a rigid, axially symmetric, ellipsoid undergoing anisotropic Brownian rotational diffusion in a continuous medium, considerably more insight can be gained. The ellipsoid spectral density has two global ($D_\parallel$ and $D_\perp$) and three local (cos α, S^2, and τ_e) parameters, the interpretation of which is clear. The average angle between the amide bond vectors and the major axis of the rotational diffusion tensor can be estimated from the ensemble of structures determined by NMR, and this allowed us to estimate the global parameters, $D_\parallel$ and $D_\perp$. We were then able to show that the ellipsoid spectral density equation can reproduce the major features of the T_1 and T_2 profiles of the three helices of the HMG1 A-domain, especially the change in baseline between helices II and III (see Figure 6). We also analyzed the data in terms of a fully anisotropic model (not shown). This analysis gave very similar results, supporting our assumption that the protein can be described as a rigid, axially symmetric, ellipsoid.

The moment of inertia I_a of an ellipsoid with radii a, b, and c is $I_a = (m/5)(b^2 + c^2)$. For prolate axial symmetry, $a > b = c$, so $I_a = (m/5)2b^2$ and $I_b = (m/5)(a^2 + b^2)$. If $I_a/I_b \cong 1/2$, then $a/b \cong \sqrt{3} = 1.73$. Using classical hydrodynamic theory (Cantor & Schimmel, 1980), this ratio of a/b gives the ratio of overall correlation times (τ_a/τ_b) as ~0.82 and the ratio of the rotational diffusion rates (D_a/D_b) as ~1.6. These values fit well with our experimentally determined values: $\tau_a/\tau_b = 0.83$ (9.0/10.8) and $D_a/D_b = 1.66$ (2.47/1.49). Overall, our analysis suggests that the structures of the A-

and B-domains of HMG1 in solution are not globular but can be approximated as rigid ellipsoids. They strengthen our belief that the structures we have determined by NMR spectroscopy are substantially correct. Further support for this conclusion comes from the structure of the HMG box from HMG-D (Jones *et al.*, 1994) which is very similar to our previously determined structure of the B-domain of HMG1 (Weir *et al.*, 1993).

Comparison of the A-Domain with the HMG Box in HMG-D and the B-Domain. Despite the overall similarities, comparison of the ^{15}N relaxation data from the A- and B-domains of HMG1 and the HMG box of HMG-D suggests some differences in the structure of these proteins. First, in both the B-domain and HMG-D, the pattern of ^{15}N T_1 and T_2 values suggests that helix I changes orientation in going from the N- to the C-terminus and that at the C-terminus its orientation is close to 180° relative to helix III; in the A-domain there is no such change, suggesting that the helix must be straighter. These results are entirely consistent with the families of structures themselves (see Figure 4); the B-domain thus appears to be more similar to HMG-D than to the A-domain. In the A-domain there is an insertion of two extra residues in the loop between helices I and II, and it is possible that the difference in orientation of helix I is related to this insertion. In the absence of this study of the backbone dynamics we would have been less sure of the significance of the differences seen in the structures themselves. With the relaxation data, however, we can be more confident that the differences seen are not, for example, due to any lack of NOEs defining the orientation of the C-terminus of helix I in the structure determination of the A-domain. Moreover, in HMG-D, the N-terminus of helix I abuts the first/second turn of helix III, but the third turn in the A- and B-domains of HMG1. This difference is likely to be related to the deletion of two residues in the loop between helices II and III in HMG-D, requiring the loss of the first turn of helix III in order to maintain the same overall structure (Jones *et al.*, 1994).

In conclusion, studies of the structure and backbone dynamics have revealed small differences between the structures of the A- and B-domains of HMG1 and the HMG box from HMG-D. These differences could be important in their slightly different DNA-binding activities (Teo *et al.*, 1995).

ACKNOWLEDGMENT

We thank Dr. Andrew Raine for help with computing the moments of inertia of HMGA, Dr. Klaus Grasser for the ^{15}N-labeled B-domain, Dr. Arthur Crawford for the suggestion of Figure 2, and our other colleagues for helpful discussions.

SUPPORTING INFORMATION AVAILABLE

^{15}N T_1s, ^{15}N T_2s, and heteronuclear NOEs for 68, out of a possible 77, residues in the A-domain at two different field strengths corresponding to ^{15}N resonance frequencies of 50.7 and 60.8 MHz and ^{15}N T_1s, ^{15}N T_2s, and heteronuclear NOEs for 67, out of a possible 70, residues in the B-domain at a ^{15}N resonance frequency of 50.7 MHz (3 pages). Ordering information is given on any current masthead page.

REFERENCES

Baker, E. N., & Hubbard, R. E. (1984) *Prog. Biophys. Mol. Biol. 44*, 97−179.
Barbato, G., Ikura, M., Kay, L. E., Pastor, R. W., & Bax, A. (1992) *Biochemistry 31*, 5269−5278.
Baxevanis, A., & Landsman, D. (1995) *Nucleic Acids Res. 23*, 1604−1613.
Borer, P. N., LaPlante, S. R., Kumar, A., Zanatta, N., Martin, A., Hakkinen, A., & Levy, G. C. (1994) *Biochemistry 33*, 2441−2450.
Cantor, C. R. C., & Schimmel, P. R. (1980) *Biophysical Chemistry,* Part II, p 549, W. H. Freeman and Co., New York.
Chen, C., Feng, Y., Short, J. H., & Wand, A. J. (1993) *Arch. Biochem. Biophys. 306*, 510−514.
Clore, G. M., Szabo, A., Bax, A., Kay, L. E., Driscoll, P. C., & Gronenborn, A. M. (1990) *J. Am. Chem. Soc. 112*, 4989−4991.
Dölle, A., & Bluhm, T. (1989) *Prog. NMR Spectrosc. 21*, 175−201.
Eriksson, M. A. L., Berglund, H., Härd, T., & Nilsson, L. (1993) *Proteins 17*, 375−390.
Faciola, L., Murchie, A. I. H., Lilley, D. M. J., & Bianchi, M. E. (1994) *Nucleic Acids Res. 22*, 285−292
Fushman, D., Weisemann, R., Thüring, H., & Rüterjans, H. (1994) *J. Biomol. NMR 4*, 61−78.
Grosschedl, R. Giese, K., & Pagel, J. (1994) *Trends Genet. 10*, 94−100.
Hansen, A. P., Petros, A. M., Meadows, R. P., & Fesik, S. W. (1994) *Biochemistry 33*, 15418−15424.
Hardman, C. H., Broadhurst, R. W., Raine, A. R. C., Grasser, K. D., Thomas, J. O., & Laue, E. D. (1995) *Biochemistry 34*, 16596−16607.
Huntress, W. T. (1968) *J. Chem. Phys. 48*, 3524−3533.
Jones, D. N. M., Searles, M. A., Shaw, G. L., Churchill, M. E. A., Ner, S. S., Keeler, J., Travers, A. A., & Neuhaus, D. (1994) *Structure 2*, 609−627.
Kay, L. E., Torchia, D. A., & Bax, A. (1989) *Biochemistry 28*, 8972−8979.
Kraulis, P. J. (1991) *J. Appl. Crystallogr. 24*, 946−950.
Kraulis, P. J., Domaille, P. J., Campbell-Burk, S. L., Van Aken, T., & Laue, E. D. (1994) *Biochemistry 33*, 3515−3531.
Landsman, D., & Bustin, M. (1993) *BioEssays 15*, 539−546.
Lipari, G., & Szabo, A. (1982) *J. Am. Chem. Soc. 104*, 4546−4559, 4559−4570.
Marion, D., Ikura, M., & Bax, A. (1989) *J. Magn. Reson. 84*, 425−430.
Ner, S. (1992) *Curr. Biol. 2*, 208−210.
Nirmala, N. R., & Wagner, G. (1988) *J. Am. Chem. Soc. 110*, 7557−7558.
Noggle, J. H., & Schirmer, R. E. (1971) *The nuclear Overhauser effect; chemical applications*, Academic Press, New York.
Palmer, A. G., III, Rance, M., & Wright, P. E. (1991) *J. Am. Chem. Soc. 113*, 4371−4380.
Press, W. H., Flannery, B. P., Teukolsky, S. A., & Vettering, W. T. (1986) *Numerical Recipes*, Cambridge University Press, Cambridge.
Read, C. M., Cary, P. D., Crane-Robinson, C., Driscoll, P. C., & Norman, D. G. (1993) *Nucleic Acids Res. 21*, 3427−3436.
Schneider, D. M., Dellwo, M. J., & Wand, A. J. (1992) *Biochemistry 31*, 3645−3652.
Smith, P. E., & Van Gunsteren, W. F. (1994) *J. Mol. Biol. 236*, 629−636.
Teo, S.-H., Grasser, K. D., & Thomas, J. O. (1995) *Eur. J. Biochem. 230*, 943−950.
van Mierlo, C. P. M., Darby, N. J., Keeler, J., Neuhaus, D., & Creighton, T. E. (1993) *J. Mol. Biol. 229*, 1125−1146.
Wagner, G. (1993) *Curr. Opin. Struct. Biol. 3*, 748−754.
Weir, H. M., Kraulis, P. J., Hill, C. S., Raine, A. R. C., Laue, E. D., & Thomas, J. O. (1993) *EMBO J. 12*, 1311−1319.
Woessner, D. T. (1962) *J. Chem. Phys. 37*, 647−654.
Zheng, Z., Czaplicki, J., & Jardetzky, O. (1995) *Biochemistry 34*, 5212−5223.

BI951404K